UC Santa Cruz
UC Santa Cruz Previously Published Works

Title

Automatic Mass Balancing of a Spacecraft Three-Axis Simulator: Analysis and Experimentation

Permalink

Journal

ISSN

Authors

Chesi, Simone
Gong, Qi
Pellegrini, Veronica
et al.

Publication Date

2014

DOI

Peer reviewed

Automatic Mass Balancing of a Spacecraft Three-Axis Simulator: Analysis and Experimentation

Simone Chesi,* Qi Gong,† and Veronica Pellegrini‡
University of California, Santa Cruz, Santa Cruz, California 95064
and
Roberto Cristi§ and Marcello Romano¶
Naval Postgraduate School, Monterey, California 93943

Spacecraft three-axis simulators provide frictionless and, ideally, torque-free hardware simulation platforms that are crucial for validating spacecraft attitude determination and control strategies. To reduce the gravitational torque, the distance between the simulator center of mass and the center of rotation needs to be minimized. This work proposes an automatic mass balancing system for spacecraft simulators, which uses only the three sliding masses during the balancing process, without need of further actuators. The proposed method is based on an adaptive nonlinear feedback control that aims to move, in real time, the center of mass toward the spacecraft simulator's center of rotation. The stability of the feedback system and the convergence of the estimated unknown parameter (the distance between the center of mass and the center of rotation) are analyzed through Lyapunov stability theory. The proposed method is experimentally validated using the CubeSat Three-Axis Simulator at the Spacecraft Robotics Laboratory of the Naval Postgraduate School.

Nomenclature

E_r	=	system rotational energy, J
E_t	=	system total energy, J
G	=	Jacobian of $[Y, DY]^T$
g^b	=	gravity vector, body-fixed coordinate system, m/s^2
g_x^b	=	x component of the gravity vector, body coordinate system, m/s^2
g_y^b	=	y component of the gravity vector, body coordinate system, m/s^2
g_z^b	=	z component of the gravity vector, body coordinate system, m/s^2
g^i	=	gravity vector, inertial-fixed coordinate system, m/s^2
H	=	measurement distribution matrix
J	=	spacecraft simulator inertia matrix, kg · m^2
J_0	=	spacecraft simulator inertia matrix before mass balancing procedure
k_p	=	arbitrary positive scalar
m_p	=	sliding masses mass, kg
$m_{s/c}$	=	spacecraft simulator mass, kg
m_x	=	sliding mass in the x^b direction
m_y	=	sliding mass in the y^b direction
m_z	=	sliding mass in the z^b direction
P_g	=	system potential energy, J
P_p	=	projection factor
P_0	=	error covariance matrix
Q	=	process covariance matrix
q	=	quaternion vector
R	=	measurement covariance matrix
R_i^b	=	rotation matrix between inertial-fixed to body-fixed coordinate system
r	=	mass balances position vector, m
r^{off}	=	center of rotation to center of mass vector, m
r_e^{off}	=	offset estimation error, m
r_x^{off}	=	x component of the center of rotation to center of mass vector, m
r_x	=	center of rotation to m_x vector, m
r_y^{off}	=	y component of the center of rotation to center of mass vector, m
r_y	=	center of rotation to m_y vector, m
r_z^{off}	=	z component of the center of rotation to center of mass vector, m
r_z	=	center of rotation to m_z vector, m
T_s	=	sample time, s
t	=	time, s
V	=	Lyapunov function
v	=	measurement noise
w	=	process noise
X	=	state vector for $[q, \omega, \tilde{\Theta}]^T$
X^i	=	x coordinate, inertial coordinate system, m
x	=	state vector for $[\omega_x, \omega_y, \omega_z, r_z^{off}]^T$
x^b	=	x coordinate, body coordinate system, m
Y	=	state vector for $[\omega]$
Y^i	=	y coordinate, inertial coordinate system, m
y^b	=	y coordinate, body coordinate system, m
Z^i	=	z coordinate, inertial coordinate system, m
z^b	=	z coordinate, body coordinate system, m
Γ	=	spacecraft simulator angular momentum, N · m · s
Θ	=	offset vector, m
$\hat{\Theta}$	=	offset estimation, m
$\tilde{\Theta}$	=	offset estimation error, m
σ	=	standard deviation
τ_r	=	theoretical control torque, N
ω	=	angular velocity vector, rad/s
ω_g	=	angular velocity vector parallel to the gravity field, rad/s
ω_p	=	angular velocity vector perpendicular to the gravity field, rad/s

*Ph.D. Candidate, Applied Mathematics and Statistics Department; schesi@soe.ucsc.edu. Member AIAA.
†Associate Professor, Applied Mathematics and Statistics Department; qigong@soe.ucsc.edu. Member AIAA.
‡Ph.D. Candidate, Applied Mathematics and Statistics Department; vpellegr@soe.ucsc.edu.
§Professor, Electrical Engineering Department; rcristi@nps.edu.
¶Associate Professor, Mechanical and Aerospace Engineering Department; mromano@nps.edu. Associate Fellow AIAA.

I. Introduction

EXPERIMENTAL test beds to simulate spacecraft dynamics, navigation, and control can greatly reduce the costs and risks

related to the design of attitude control and determination systems for small spacecraft [1]. A three-axis simulator consists of a hollow hemispherical air bearing, floating over a correspondent hemispherical cup through which compressed air is flowing. The air-bearing hemisphere contains sensors, actuators, computers, and power storage/conditioning to fully model a spacecraft attitude determination and control system. The simulator enables full three-degree-of-freedom rotational motion for attitude dynamics and control simulations [2]. To simulate a frictionless and torque-free environment for rigorous ground testing of spacecraft systems, disturbance torques must be compensated. The major disturbance torque that spoils the rigorous reproduction of a torque-free space environment is due to gravity [3]. To minimize this disturbance torque, the distance between the center of mass and the center of rotation needs to be minimized. A standard procedure for manually balancing a spacecraft simulator is described in [4], where, by inspecting the spacecraft simulator pendulum motion, the balance masses are moved to increase the period of the pendulum motion. This method requires multiple trials and is limited in real applications because of the rotational travel constraints of the spherical air bearing. As shown in [5], by analyzing different points of equilibrium, it is possible to determinate the relationship between the spacecraft center of mass and the known positions of the balance masses. However, this method requires a considerable amount of time and does not guarantee the correct estimation of the center of mass. Manual balancing has also been implemented in [6], where the disturbance gravitational torque has been reduced to 0.01 Nm.

An automatic mass balancing system is highly desirable for spacecraft simulators, particularly during the design process, because the simulators may be subjected to modifications or upgrades. In fact, even a slight modification or relocation of the system components requires a rerun of the manual balancing procedure, which is a time-consuming process. Automatic mass balancing systems, on the other hand, can significantly reduce the balancing time from hours to possibly minutes. To overcome the limitations of manual balancing system, a number of spacecraft simulators have been equipped with an automatic balancing system [7–11]. An automatic mass balancing system was proposed by Kim and Agrawal [7], where external control moment gyros were used to track the angular momentum and determine the positions of three proof masses. Experiments on an automatic mass balancing technique were conducted in [10], where the system moves the balance masses to compensate the imbalance derived from the difference in total impulse exerted by the actuators during limit cycle. There are also automatic mass balancing systems that have been designed based on least-squares estimation of the center of mass [12–14]. The limitation of such least-squares-based techniques is that the estimation and compensation process must be repeated several times before accurate balancing is achieved.

This paper presents an automatic mass balancing technique, which uses exclusively three balance masses without any other actuators. The proposed automatic balancing system is based on adaptive nonlinear feedback control that significantly and automatically reduces the gravitational disturbance torque by a precise collocation of the center of mass on the center of rotation. The automatic mass balancing system is composed of three balance masses that are moved by electric motors along the three orthogonal directions of the body coordinate system. By assumption, the body coordinate system is aligned with the spacecraft simulator's principal inertia axes with the origin located in the spacecraft simulator's center of rotation (CR) as shown in Fig. 1. The vector $r^{\text{off}} = [\ r_x^{\text{off}} \quad r_y^{\text{off}} \quad r_z^{\text{off}}\ ]^T$ represents the unknown offset between the CR and the center of mass (CM). The goal of the automatic mass balancing system is to eliminate the unknown offset by moving the three balance masses m_x, m_y, and m_z in an appropriate manner.

With respect to other automatic balancing systems, the main advantage of the proposed system is that it does not require any other actuators besides balance masses to balance the spacecraft simulator. This aspect is particularly important when dealing with small spacecraft simulators, because actuators, such as reaction wheels or control moment gyros, require a consistent amount of volume and weight. Moreover, the proposed automatic balancing system is
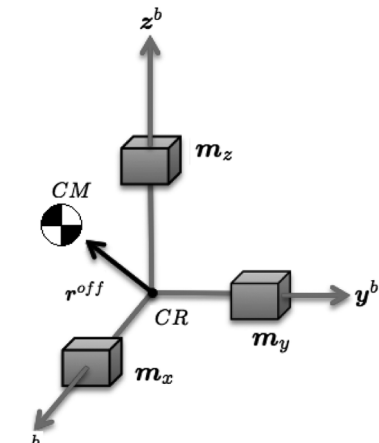

Fig. 1   Automatic mass balancing system.

simple to implement, because only three sliding masses moved by three motors are needed.

The proposed automatic balancing idea requires a control algorithm that automatically adjusts the location of the sliding masses to eliminate the unknown offset between the center of rotation and center of mass. There are some challenges that need to be successfully addressed. First, the torque that can be generated by the actuators (the balance masses) is physically confined in the direction perpendicular to the gravity field. It implies that the offset along the gravity field is very difficult to be compensated using sliding masses. For example, suppose the spacecraft is balanced in the two directions perpendicular to the gravity field, and the spacecraft is spinning along the direction of the gravity field. In such situation, the location of the sliding mass on the direction of the gravity field does not affect the motion. Therefore, the control system has very limited feedback information to use. To overcome this challenge, a two-step design has been chosen. In the first step, the offset in the transversal direction is compensated using an adaptive nonlinear control law. Once the offset in the two directions perpendicular to the gravity field are compensated, the offset in the last direction is estimated using a Kalman filter and then compensated according to the estimated offset.

In the first step of the automatic balancing procedure (i.e., compensation of offset in the directions perpendicular to the gravity field), due to the presence of unknown parameters (the components of the distance vector between the spacecraft simulator's center of mass and the center of rotation), a nonlinear adaptive control is adopted. Conceptually speaking, the proposed control algorithm is based on the conservation of the angular momentum. If the spacecraft simulator is perfectly balanced, the angular momentum is conserved because there is no acting external torque. Conversely, if an offset is present between the center of mass and the center of rotation, the angular momentum is not conserved due to the gravitational torque. This information can be used by the control system to relocate the positions of the three sliding masses until the derivative of the angular momentum is zero. The proposed nonlinear adaptive control law is proven to be stable in the sense of Lyapunov. Furthermore, by using LaSalle's invariance principle, it has been proven that the offsets along the two directions perpendicular to the gravity field can be completely compensated. In the second step, the vertical offset is estimated by an unscented Kalman filter and then compensated. The proposed automatic mass balancing system is tested on a newly developed spacecraft simulator at the Spacecraft Robotics Laboratory at the Naval Postgraduate School [15]. The purpose of this apparatus is to simulate the attitude dynamics of a class of small satellites: CubeSats. The simulation and experimental results are in strong agreement with the theoretical analysis and demonstrate a significant reduction of the disturbance torque.

The paper is organized as follows. The first step of the balancing procedure is described in Sec. II. This step uses a nonlinear adaptive control law to compensate the transversal imbalance. The vertical

imbalance compensation based on estimation techniques is considered in Sec. III. Section IV presents the simulation results, and the experimental results on the spacecraft simulator are presented in Sec. V. Finally, Sec. VI states the conclusions of this work.

II.   Transversal Imbalance Compensation

A.   System Dynamic Model

The spacecraft simulator kinematics and dynamics can be modeled using two coordinate systems as shown in Fig. 2: the inertial coordinate systems X^i, Y^i, Z^i and a coordinate system fixed to the simulator body x^b, y^b, z^b. Both coordinate systems have their origins in the center of rotation. The orientation of the body-fixed coordinate system with respect to the inertial coordinate system defines the attitude of the spacecraft simulator.

The spacecraft three-axis simulator can rotate freely, but cannot translate, because the CR is a fixed point in the inertial coordinate system. Each balance mass is assumed to be an ideal mass particle that can be translated along its corresponding axis. The rotational kinematics using a quaternion can be describe by

$$\begin{bmatrix} \dot{q}_1 \\ \dot{q}_2 \\ \dot{q}_3 \\ \dot{q}_4 \end{bmatrix} = \frac{1}{2} \begin{bmatrix} 0 & \omega_z & -\omega_y & \omega_x \\ -\omega_z & 0 & \omega_x & \omega_y \\ \omega_y & -\omega_x & 0 & \omega_z \\ -\omega_x & -\omega_y & -\omega_z & 0 \end{bmatrix} \begin{bmatrix} q_1 \\ q_2 \\ q_3 \\ q_4 \end{bmatrix} \qquad (1)$$

where $\boldsymbol{\omega} = [\omega_x \quad \omega_y \quad \omega_z]^T$ represents the absolute angular velocity of the simulator along the body coordinate system, and $\boldsymbol{q} = [q_1 \quad q_2 \quad q_3 \quad q_4]^T$ are the quaternions.

It is assumed that the system subjects to no external control torque except for the gravity torque due to the system imbalance. Assuming the balance masses are held in their original positions, the rotational dynamics of the simulator with respect to the center of rotation is given by Euler's equation [16]

$$\dot{\boldsymbol{\Gamma}} + \boldsymbol{\omega} \times \boldsymbol{\Gamma} = \boldsymbol{r}^{\text{off}} \times m_{s/c} \boldsymbol{g}^b \qquad (2)$$

where $m_{s/c}$ is the simulator mass including the three proof masses, and $\boldsymbol{\Gamma}$ is the angular momentum, which can be written as

$$\boldsymbol{\Gamma} = \boldsymbol{J}\boldsymbol{\omega} \qquad (3)$$

with $\boldsymbol{J}$ as the simulator inertia matrix. By assumption, the body coordinate system is parallel to the principal inertia axes of the simulator, hence the inertia matrix is diagonal. Additionally, it has been assumed that the three balance masses are aligned with the axes of principal inertia and that they have the same mass m_p. The inertia matrix can then be written as

$$\boldsymbol{J} = \boldsymbol{J}_0 - m_p \sum_i [\boldsymbol{r}_i \times][\boldsymbol{r}_i \times] \quad \text{for } i = x, y, z \qquad (4)$$

where $\boldsymbol{J}_0$ is the inertia matrix before the balancing procedure, and the vector $\boldsymbol{r}_i$ represents the position of the ith balance mass with respect
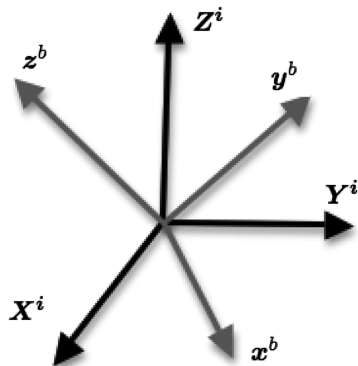

Fig. 2   Inertial and body coordinate systems.

to the CR. Furthermore, due to the small entity of the masses and the low speed of their motion, it has been assumed that the effect of the motion of the balancing masses on the angular momentum can be neglected. In Eq. (4), $[\boldsymbol{r}_i \times]$ is a cross-product matrix defined as

$$[\boldsymbol{r}\times] = \begin{bmatrix} 0 & -r_3 & r_2 \\ r_3 & 0 & -r_1 \\ -r_2 & r_1 & 0 \end{bmatrix} \quad \text{with} \quad \boldsymbol{r} = \begin{bmatrix} r_1 \\ r_2 \\ r_3 \end{bmatrix} \qquad (5)$$

To balance the spacecraft simulator, the Earth gravitational field $\boldsymbol{g}^b$ in the body coordinate system must be computed using the simulator attitude through the direction cosine matrix

$$\boldsymbol{g}^b = \boldsymbol{R}_i^b \boldsymbol{g}^i \qquad (6)$$

where $\boldsymbol{g}^i = [0 \quad 0 \quad -9.81]^T$ m/s^2 is the gravitational field in the inertial coordinate system, and $\boldsymbol{R}_i^b$ is the rotation matrix defined as

$$\boldsymbol{R}_i^b = \begin{bmatrix} 1 - 2(q_2^2 + q_3^2) & 2(q_1 q_2 - q_4 q_3) & 2(q_1 q_3 + q_4 q_2) \\ 2(q_1 q_2 + q_4 q_3) & 1 - 2(q_1^2 + q_3^2) & 2(q_2 q_3 - q_4 q_1) \\ 2(q_1 q_3 - q_4 q_2) & 2(q_1 q_3 + q_4 q_1) & 1 - 2(q_1^2 + q_2^2) \end{bmatrix}$$
$$(7)$$

The purpose of this paper is to use the sliding masses to relocate the CM of the spacecraft simulator toward the CR to eliminate the gravitational torque. The proposed method assumes that the simulator inertia matrix is known and constant. In the next sections, a two-step design is presented. In the first step, the two transversal directions x^b and y^b are balanced by using an adaptive nonlinear feedback control; in the second step, the imbalance in the remaining direction is estimated by using an unscented Kalman filter, and then the offset is compensated. The main reason for such a two-step design is that the torque generated by the moving masses is always constrained in a plane orthogonal to the gravitational field, which greatly limits the control space and generates difficulties in feedback control design.

B.   Adaptive Nonlinear Feedback Control Law

The proposed adaptive control technique is based on the conservation of the angular momentum. If the gravitational torque is zero, the angular momentum is conserved. However, in the presence of an offset between CM and CR, and therefore of a gravitation torque, the angular momentum is not conserved. The main concept of the proposed imbalance compensation method is to impose that the derivative of the angular momentum become zero by displacing, in real time, the three balance masses.

The mechanical control generated by moving the balance masses can be expressed as

$$\boldsymbol{\tau}_r = m_p \sum_i \boldsymbol{r}_i \times \boldsymbol{g}^b \quad \text{for } i = x, y, z \qquad (8)$$

where $\boldsymbol{r}_i$, the ith balance mass's position with respect to the CR, is the control input to be designed.[**] By considering Eq. (2) and taking into consideration the effect of $\boldsymbol{\tau}_r$, the system dynamics can be written as

$$\dot{\boldsymbol{\Gamma}} + \boldsymbol{\omega} \times \boldsymbol{J}\boldsymbol{\omega} = \boldsymbol{r}^{\text{off}} \times m_{s/c} \boldsymbol{g}^b + \boldsymbol{\tau}_r \qquad (9)$$

In this formulation, the torque $\boldsymbol{\tau}_r$ will be treated as the dummy control to be designed using nonlinear adaptive control. Then, the real control $\boldsymbol{r}_i$ will be designed to generate the desired control torque. However, from Eq. (8), clearly the torque generated by moving the

---

[**]Notably, the effect of the displacement of the three equal masses, sliding each in one direction, on the generation of the gravitational torque, is the same that it would be obtained by using a single mass displaced in three dimensions by the sum of the displacement vectors of the three masses. However, using three masses has the advantage of leaving diagonal the matrix of principal inertia with respect to the center of rotation.

masses is constrained in the plane orthogonal to g^b. This infers that, in the design of the control torque τ_r, it needs to contain no component along the vector g^b.

To design the theoretical torque τ_r, let $\boldsymbol{\Theta} = r^{\text{off}}$, where the parameter r^{off} represents the unknown and time-invariant initial offset between the center of mass and the center of rotation. Then,

$$\boldsymbol{\Theta} \times m_{\text{s/c}} g^b = \boldsymbol{\Phi}\boldsymbol{\Theta} \tag{10}$$

with

$$\boldsymbol{\Phi}(q) = -m_{\text{s/c}} g^b \times \tag{11}$$

Let $\hat{\boldsymbol{\Theta}}(t)$ be the estimation of the unknown vector parameter $\boldsymbol{\Theta}$, and define the estimation error $\hat{\boldsymbol{\Theta}}(t)$ as

$$\tilde{\boldsymbol{\Theta}}(t) = \boldsymbol{\Theta} - \hat{\boldsymbol{\Theta}}(t) \tag{12}$$

The dynamics of $\hat{\boldsymbol{\Theta}}(t)$ will be determined later through Lyapunov analysis.

Define the state vector for the overall problem as $X = [q, \omega, \tilde{\boldsymbol{\Theta}}]^T$ The angular velocity vector ω can be decomposed into two components, one ω_g along the vector g^b and the other ω_p, orthogonal to g^b, that is,

$$\omega = \omega_g + \omega_p, \qquad \omega_g^T \omega_p = 0, \qquad (g^b)^T \omega_p = 0 \tag{13}$$

Let us also define the projection operator

$$P_p(q) = \left[I - \frac{g^b (g^b)^T}{\|g^b\|^2} \right] \tag{14}$$

so that

$$\omega_p = P_p(q)\omega \tag{15}$$

where ω_p represents the angular velocity perpendicular to the Earth's gravitational field.

To design the state feedback control and the adaptive law for $\hat{\boldsymbol{\Theta}}$, the following positive definite Lyapunov function is used:

$$V(q, \omega, \tilde{\boldsymbol{\Theta}}) = \tfrac{1}{2}\omega^T J \omega + \tfrac{1}{2}\tilde{\boldsymbol{\Theta}}^T \tilde{\boldsymbol{\Theta}} + \tfrac{1}{2} q^T q \tag{16}$$

The time derivative of the Lyapunov function along the motion of the system leads to

$$\begin{aligned} \dot{V}(t) &= \omega^T J \dot{\omega} + \tilde{\boldsymbol{\Theta}}^T \dot{\tilde{\boldsymbol{\Theta}}} + q^T \dot{q} \\ &= \omega^T (-\omega \times J\omega + \boldsymbol{\Phi}\boldsymbol{\Theta} + \tau_r) + \tilde{\boldsymbol{\Theta}}^T \dot{\tilde{\boldsymbol{\Theta}}} \\ &= \omega^T \boldsymbol{\Phi}\boldsymbol{\Theta} + \omega^T \tau_r + \tilde{\boldsymbol{\Theta}}^T \dot{\tilde{\boldsymbol{\Theta}}} \end{aligned} \tag{17}$$

where Eqs. (9) and (11) have been used, together with the hypothesis of constant J. From Eqs. (12) and (17) became

$$\dot{V} = \omega^T \boldsymbol{\Phi}\hat{\boldsymbol{\Theta}} + \tilde{\boldsymbol{\Theta}}^T (\boldsymbol{\Phi}^T \omega + \dot{\tilde{\boldsymbol{\Theta}}}) + \omega^T \tau_r \tag{18}$$

Let the adaptive law for the estimated parameter be

$$\dot{\hat{\boldsymbol{\Theta}}} = \boldsymbol{\Phi}^T \omega \tag{19}$$

and the control torque be

$$\tau_r = -\boldsymbol{\Phi}\hat{\boldsymbol{\Theta}} - k_p \omega_p \tag{20}$$

where the parameter k_p is an arbitrary positive scalar. Substituting Eqs. (19) and (20) into Eq. (18), obtaining

$$\begin{aligned} \dot{V} &= \omega^T \boldsymbol{\Phi}\hat{\boldsymbol{\Theta}} - \omega^T \boldsymbol{\Phi}\hat{\boldsymbol{\Theta}} - k_p \omega^T \omega_p \\ &= -k_p \omega^T \omega_p \\ &= -k_p (\omega_g + \omega_p)^T \omega_p \end{aligned} \tag{21}$$

Since $\omega_g^T \omega_p = 0$, this yields

$$\dot{V} = -k_p \|\omega_p\|^2 \tag{22}$$

From Eq. (22), it is possible to see that the derivative of the Lyapunov function is negative semidefinite, hence the closed-loop control system is Lyapunov stable. Moreover, by the LaSalle invariance principle [17], the system will converge to the largest invariant set Ω contained in

$$\{\dot{V}(t) \equiv 0\} = \{X : \dot{V}(q, \omega, \tilde{\boldsymbol{\Theta}}) \equiv 0\} = \{\omega_p(t) \equiv 0\} \tag{23}$$

in other words, $\lim_{t \to \infty} \omega_p(t) = 0$.

C. Control Torque Generation

The designed theoretical control torque τ_r must be physically created by moving the balance masses. The torque generated by the sliding masses is constrained to a direction normal to both the masses' position vector and the gravitational field direction. If τ_r is designed according to Eq. (20), this property can be guaranteed. In fact, multiplying $(g^b)^T$ to both sides of Eq. (20), and using Eqs. (11) and (13), leads to

$$(g^b)^T \tau_r = -(g^b)^T \boldsymbol{\Phi}\hat{\boldsymbol{\Theta}} - k_p (g^b)^T \omega_p = 0 \tag{24}$$

To design the real control r, which is the balance masses' position vector, the designed torque τ_r needs to be mapped to r. For this purpose, substituting τ_r in Eq. (8) gives

$$\tau_r = m_p(-g^b(t) \times r) \tag{25}$$

Because the matrix $[-g^b(t)\times]$ is always singular, r cannot be directly found by inverting it. However, due to property (24), the designed control torque τ_r is guaranteed to be in the range of $[-g^b(t)\times]$ for all t, so that Eq. (25) always has a solution for r. Indeed, a solution is given by

$$r = \frac{g^b \times \tau_r}{\|g^b\|^2 m_p} \tag{26}$$

To see this, substituting Eq. (26) into Eq. (25), and using the condition $g^b \perp \tau_r$, $\forall$ t from Eq. (24), it can be found that

$$-m_p \left(\frac{g^b \times g^b \times \tau_r}{\|g^b\|^2 m_p} \right) = -m_p \left(\frac{(g^b \cdot \tau_r)g^b - (g^b \cdot g^b)\tau_r}{\|g^b\|^2 m_p} \right) = \tau_r \tag{27}$$

Therefore, the control applied to the mass balancing system is given by Eq. (26) with τ_r be designed according to Eq. (20).

D. Convergence of the Estimated Parameters

By the LaSalle invariance principle [17], the system will converge to the largest invariant set Ω contained in Eq. (23). On the set $\{\omega_p(t) \equiv 0\}$, the designed parameters estimation law in Eq. (19) leads to

$$\dot{\hat{\boldsymbol{\Theta}}} = \boldsymbol{\Phi}^T \omega = \boldsymbol{\Phi}^T \omega_p + \boldsymbol{\Phi}^T \omega_g = \boldsymbol{\Phi}^T \omega_g = 0 \tag{28}$$

because ω_g is always orthogonal to all columns of $\boldsymbol{\Phi}$, which represents the cross-product matrix form of the gravity field.

On the set $\{\omega_p(t) \equiv 0\}$, the spacecraft remains to spin with an angular velocity aligned to the gravity field. This condition is shown in Fig. 3, where it has been assumed that the spacecraft remains to
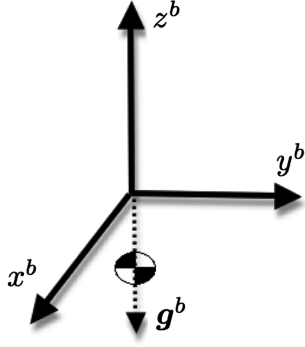
Fig. 3 Spacecraft simulator z^b axis aligned with g^b.

rotate around the z^b axis. Under this condition, it is possible to prove the convergence of the parameter. Indeed, the closed-loop dynamics can be obtained by replacing the control actions into Eq. (2) so that

$$\dot{\omega} = J^{-1}(-\omega \times J\omega + \Phi\tilde{\Theta} - k_p\omega_p) \qquad (29)$$

The projection factor P_p in Eq. (14), can be written as

$$P_p(q) = \begin{bmatrix} 1 & 0 & 0 \\ 0 & 1 & 0 \\ 0 & 0 & 1 \end{bmatrix} - \begin{bmatrix} (g_x^b)^2 & g_x^b g_y^b & g_x^b g_z^b \\ g_y^b g_x^b & (g_y^b)^2 & g_y^b g_z^b \\ g_z^b g_x^b & g_z^b g_y^b & (g_z^b)^2 \end{bmatrix} \frac{1}{\|g^b\|} \qquad (30)$$

Because on the set Ω, $\omega_p(t) \equiv 0$, the spacecraft simulator is rotating around the gravity field along the z^b axis so that the components g_x^b, g_y^b of the projection factor go to zero. As a consequence,

$$P_p(q) = \begin{bmatrix} 1 & 0 & 0 \\ 0 & 1 & 0 \\ 0 & 0 & 0 \end{bmatrix} \qquad (31)$$

Premultiplying Eq. (29) by the projection factor P_p leads to

$$P_p\dot{\omega} = \frac{d(P_p\omega)}{dt} = \dot{\omega}_p = P_p J^{-1}(-\omega \times J\omega + \Phi\tilde{\Theta} - K_p\omega_p) \quad (32)$$

where the time derivative of the projection factor is equal to zero only on the set $\{\omega_p(t) \equiv 0\}$. Since $\omega = \omega_g + \omega_p$ on $\{\omega_p \equiv 0\}$, Eq. (32) becomes

$$0 = P_p J^{-1}(-\omega_g \times J\omega_g + \Phi\tilde{\Theta}) \qquad (33)$$

Because J is diagonal and ω_g has only one component along the z^b axis, it can be shown that $\omega_g \times J\omega_g = 0$. Therefore, Eq. (33) becomes

$$0 = P_p J^{-1}(\Phi\tilde{\Theta}) \qquad (34)$$

where the matrix Φ can be written, from Eq. (11), as

$$\Phi = m_{s/c} \begin{bmatrix} 0 & g_z^b & 0 \\ -g_z^b & 0 & 0 \\ 0 & 0 & 0 \end{bmatrix} \qquad (35)$$

And so, Eq. (34) can be written as

$$0 = m_{s/c} \begin{bmatrix} 1 & 0 & 0 \\ 0 & 1 & 0 \\ 0 & 0 & 0 \end{bmatrix} \begin{bmatrix} J_{xx}^{-1} & 0 & 0 \\ 0 & J_{yy}^{-1} & 0 \\ 0 & 0 & J_{zz}^{-1} \end{bmatrix} \begin{bmatrix} 0 & g_z^b & 0 \\ -g_z^b & 0 & 0 \\ 0 & 0 & 0 \end{bmatrix} \begin{bmatrix} \tilde{\Theta}_x \\ \tilde{\Theta}_y \\ \tilde{\Theta}_z \end{bmatrix} \qquad (36)$$

which yields

$$J_{xx}^{-1} \cdot g_z^b \cdot \tilde{\Theta}_y = 0 \quad -J_{yy}^{-1} \cdot g_z^b \cdot \tilde{\Theta}_x = 0 \quad 0 \cdot \tilde{\Theta}_z = 0 \qquad (37)$$

Since J_{xx}^{-1}, J_{yy}^{-1}, $g_z^b \neq 0$, Eq. (37) implies $\tilde{\Theta}_x = \tilde{\Theta}_y = 0$. Thus, r_x^{off}, r_y^{off} have been correctly estimated and compensated. In fact, by considering Eqs. (20) and (23), the right-hand side of Eq. (9) is equal to zero and this implies that no gravitational torque is acting on the spacecraft (i.e., the distance between CM and CR has been compensated at least in two directions). But nothing can be claimed about the third component of $\tilde{\Theta}$. This component will be estimated using a Kalman filter as demonstrated in the following section.

III. Vertical Imbalance Compensation

Once the offsets along r_x^{off} and r_y^{off} directions are balanced, the offset in the remaining z^b direction needs to be compensated. Spacecraft attitude and parameter estimation has been studied using the extended Kalman filter (EKF) and unscented Kalman filter (UKF) [18–21]. For the dynamic system described in Eq. (2), either UKF or EKF can be used, and the performance is expected to be similar. In this study, the UKF is used to estimate the offset r_z^{off} by a standard approach of augmenting this unknown parameter into the state space [22].

To write the system in state-space form, let us define the state vector of the continuous system as $x = [\omega_x, \omega_y, \omega_z, r_z^{\text{off}}]^T$. Here, the unknown parameter r_z^{off} is augmented into the state with the corresponding dynamics to be $\dot{r}_z^{\text{off}} = 0$. The disturbance torque due to the imbalance along the z^b axis is

$$r^{\text{off}} \times m_{s/c} g^b = [-m_{s/c} g_y^b r_z^{\text{off}}, _{s/c} g_x^b r_z^{\text{off}}, 0]^T \qquad (38)$$

Therefore, the spacecraft simulator dynamics in the state-space form is given by

$$\dot{x} = f(x) + d(t) \qquad (39)$$

where

$$f = \begin{bmatrix} J^{-1}\left(-\omega \times J\omega + \begin{bmatrix} -m_{s/c} \cdot g_y^b \cdot r_z^{\text{off}} \\ m_{s/c} \cdot g_x^b \cdot r_z^{\text{off}} \\ 0 \end{bmatrix} \right) \\ 0 \end{bmatrix} \qquad (40)$$

and $d(t)$ represents the process noise. Let the measurement be the angular velocity given by the inertial measurement unit (IMU). Then the output equation is given by $y = Hx + v(t)$, where

$$H = \begin{bmatrix} 1 & 0 & 0 & 0 \\ 0 & 1 & 0 & 0 \\ 0 & 0 & 1 & 0 \end{bmatrix} \qquad (41)$$

and $v(t)$ represents the measurement noise.

To correctly estimate the offset in the last direction using the UKF, the observability of the unknown parameter needs to be analyzed. In this paper, the definition of observability for the nonlinear system introduced in [23] has been adopted. Consider a general nonlinear system

$$\dot{\xi} = f(t, \xi, u), \qquad \xi \in R^n, \qquad u \in R^m \quad Y = h(t, \xi, u) \quad (42)$$

where ξ is the state, $u(t)$ is a continuous control input, and Y represents the variable that can be directly measured by sensors. Suppose $z = z(t, \xi, u)$ is a variable to be estimated. Let U represent an open and connected set in the time-state-control space $R \times R^n \times R^m$.

Definition 1 (Observability) [23]: The function $z = z(t, \xi(t), u(t))$ is said to be observable in U if for any two trajectories $(t, \xi^i(t), u^i(t))$, $i = 1, 2$ in U defined on a same interval $[t_0, t_1]$, the equality

$$h(\xi^1(t), u^1(t)) = h(\xi^2(t), u^2(t)), \qquad \text{a.e. in } [t_0, t_1] \quad (43)$$

implies

$$z(t, \xi^1(t), u^1(t)) = z(t, \xi^2(t), u^2(t)) \qquad (44)$$

almost everywhere in $[t_0, t_1]$. Suppose for any trajectory $(t, \xi(t), u(t))$ in U there always exists an open set $U_1 \subset U$ so that $(t, \xi(t), u(t))$ is contained in U_1 and $z(t, \xi, u)$ is observable in U_1. Then, $z = z(t, \xi, u)$ is said to be locally observable in U.

Lemma 1 [23]: Consider a system without control

$$\dot{\xi} = f(t, \xi), \qquad \xi \in \Re^n \quad Y = h(t, \xi) \qquad (45)$$

Let $U \subset \Re \times \Re^n$ be an open set. Consider

$$V = (Y^T, DY^T, \ldots \ldots, D^{l-1}Y^T)^T \qquad (46)$$

for some $l > 0$, where D is the differentiation operator. If

$$\text{rank}\left(\frac{\partial V}{\partial \xi}\right) = n$$

for $(t, \xi) \subset U$, then $z = z(t, \xi)$ is locally observable in U.

The aforementioned observability definition and Lemma are applied to the spacecraft simulator dynamics in Eq. (40) with measurement $h(t) = [\omega_x, \omega_y, \omega_z]$. The variable to be estimated is $z(t, \xi) = r_z^{\text{off}}$. By denoting the differentiation operator D, then

$$Y = [\boldsymbol{\omega}]$$

$$DY = [\dot{\boldsymbol{\omega}}] = \left[J^{-1}\left(-\boldsymbol{\omega} \times J\boldsymbol{\omega} + \begin{bmatrix} -m_{s/c} \cdot g_y^b \cdot r_z^{\text{off}} \\ m_{s/c} \cdot g_x^b \cdot r_z^{\text{off}} \\ 0 \end{bmatrix}\right) \right] \quad (47)$$

According to Lemma 1, if the Jacobian of $[Y, DY]^T$, that is,

$$G = \frac{\partial}{\partial X}\begin{bmatrix} Y \\ DY \end{bmatrix} \qquad (48)$$

has full rank, then local observability can be guaranteed. The Jacobian matrix has the following triangular structure:

$$G = \begin{bmatrix} I_{3\times3} & 0_{3\times1} \\ G_{21} & G_{22} \end{bmatrix} \qquad (49)$$

where $I_{3\times3}$ is the (3×3) identity matrix, G_{21} is a (3×3) matrix, and G_{22} is a 3×1 vector given by

$$G_{22} = \frac{\partial\dot{\boldsymbol{\omega}}}{\partial r_z^{\text{off}}} = \begin{bmatrix} -\frac{m_{s/c}g_y^b}{J_{xx}} \\ -\frac{m_{s/c}g_x^b}{J_{yy}} \\ 0 \end{bmatrix} \qquad (50)$$

Hence, the Jacobian matrix G has full column rank (i.e., the system is locally observable), if $[g_y^b, g_x^b] \neq [0, 0]$. This condition can be satisfied if the simulator is tumbling under the gravity torque. For this reason, to estimate the unknown parameter r_z^{off}, initially the simulator has been put in a tumbling motion by giving it an angular velocity with components in all three directions. After r_z^{off} has been estimated, the balance mass m_z can be moved along the z^b axis to compensate the offset in that direction, thus concluding the automatic balancing in all three directions.

IV. Simulation Results

The simulation results shown here validate the effectiveness of the balancing procedure proposed earlier. All the simulations are developed using MATLAB/Simulink 7.0 using the Runge–Kutta fourth-order integrator with fixed step $T_s = 0.05$ s. The physical parameters used for this simulation are based on the real parameters of the CubeSat three-axes simulator (CubeTAS) developed at the Spacecraft Robotics Laboratory at the Naval Post-

graduate School. The spacecraft simulator inertia matrix is $J = \text{diag}(0.0226, 0.0257, 0.0266)$ kg $\cdot$ m^2. The total mass is $m_{s/c} = 4.2$ kg with the balance masses $m_x = m_y = m_z = 0.3$ kg. An offset is simulated with values $\boldsymbol{r}^{\text{off}} = [1 - 0.9 - 1.4]^T \cdot 10^{-3}$ m, the initial angular velocity $\boldsymbol{\omega} = [0.0888 \quad 0.8229 \quad 1.3611]^T$ rad/s, and quaternion $\boldsymbol{q} = [0 \quad 0 \quad 0 \quad 1]^T$. In the simulation, the sliding masses are used as actuators. The feedback control law in Eq. (20) is generated using the simulated data of angular velocity, gravity field, and quaternions. Furthermore, the simulation assumes that the data related to the gravity field, angular velocity, and quaternions have the same sample time $T_s = 0.05$ s. The maximum translation distance for each sliding mass is ±28 mm providing a total offset compensation capability of ±2 mm in each direction. The uncertainty in the sliding masses' positions has been modeled using Gaussian white noise distribution with standard deviation $\sigma = 0.5 \cdot 10^{-6}$ m. More details on the CubeTAS simulator are presented in Sec. V.

In the first step of the proposed automatic balancing procedure, the adaptive control designed in Sec. II is applied to eliminate the transversal imbalance. The simulation results are demonstrated in Figs. 4–6. Figure 4 shows the balance masses' positions during the balancing procedure. As a physical constraint, the sliding masses' displacements need to be less than the maximum travel distance of 28 mm for all time. For this reason, the feedback gain k_p in Eq. (20) is
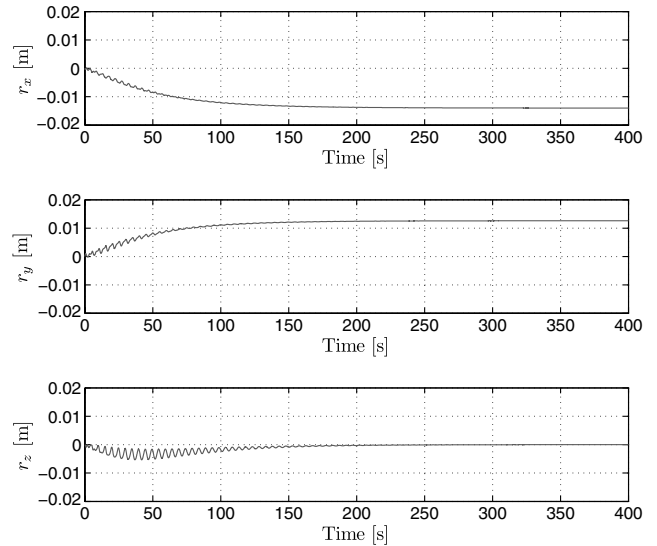

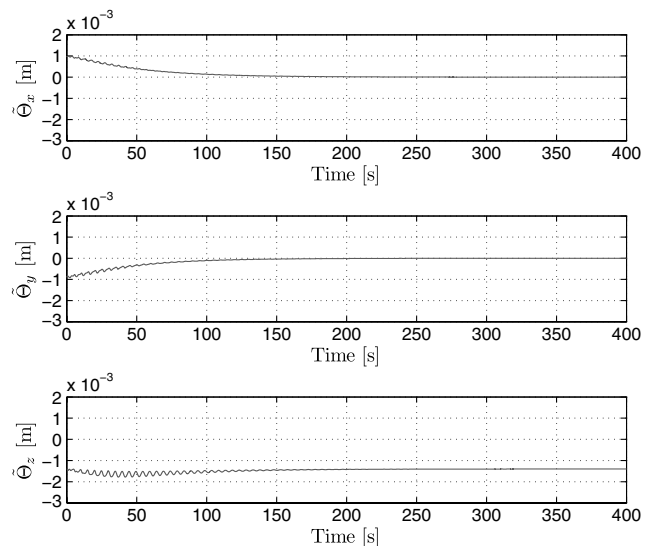Fig. 4 Simulation results: balance masses' positions.

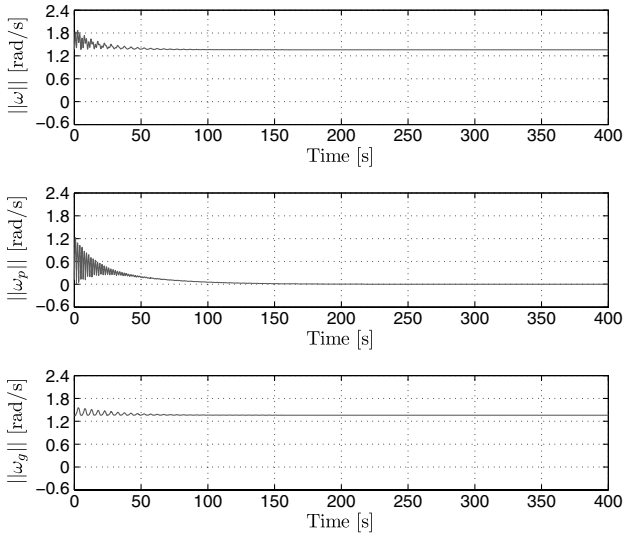Fig. 5 Simulation results: convergence of the estimated offsets.

Fig. 6 Simulation results: magnitude of ω, ω_p and ω_g during transversal balancing procedure.

tuned in a way that the sliding mass travel distance is always less than its maximum value, as shown in Fig. 4.

As shown in Fig. 5, during the mass balancing procedure, $\tilde{\Theta}_x$ and $\tilde{\Theta}_y$ converge to zero, implying that the offsets in x^b and y^b directions are balanced. $\tilde{\Theta}_z$ does not converge to zero, because the offset in the third direction r_z^{off} cannot be balanced with the proposed adaptive control. These simulation results agree with our analysis presented in preceding sections. Figure 6 shows the behavior of the angular velocity during the first step of the balancing procedure. The angular velocity perpendicular to the gravity field ω_p tends to zero and $\omega \to \omega_g$. Thus, the spacecraft remains to spin along the gravity vector as proven in Sec. II using Lyapunov stability analysis.

Once the first step is completed, the offset in the directions perpendicular to the gravity field has been compensated. The offset in the last direction r_z^{off} can be estimated in the second step. At the beginning of the second step, an angular velocity with components in all directions is applied to the spacecraft simulator. This guarantees the observability of the unknown parameter r_z^{off} as explained in Sec. III. During the rotational motion, a UKF is adopted to estimated r_z^{off}. The associated measurement and process covariance matrices, considering the hardware setup, have been chosen as

$$\boldsymbol{R} = E(\boldsymbol{vv}^T) = \text{diag}((4.87 \times 10^{-5})^2, (4.87 \times 10^{-5})^2, \\ (4.87 \times 10^{-5})^2)[\text{rad}^2/\text{s}^2] \quad (51)$$

$$\boldsymbol{Q} = E(\boldsymbol{dd}^T) = \text{diag}(10^{-10}, 10^{-10}, 10^{-10}, (1 \times 10^{-4})^2) \\ \times [\text{rad}^2/\text{s}^4, \text{rad}^2/\text{s}^4, \text{rad}^2/\text{s}^4, \text{m}^2/\text{s}^2] \quad (52)$$

The initial error covariance matrix P_0, reflecting the uncertainties in the initial estimated state variables, is set to be a diagonal matrix as

$$P_0 = \text{diag}((0.1)^2, (0.1)^2, (0.1)^2, (1.5 \times 10^{-3})^2) \\ [\text{rad}^2/\text{s}^2, \text{rad}^2/\text{s}^2, \text{rad}^2/\text{s}^2, \text{m}^2] \quad (53)$$

The simulation results using the preceding gain matrices are shown in Fig. 7, where the error between r_z^{off} and its estimation has been defined as

$$r_e^{\text{off}} = \|r_z^{\text{off}} - \hat{r}_z^{\text{off}}\| \quad (54)$$

It can be seen that the filter converges to the correct value of r_z^{off} in less than 20 s. Indeed, r_e^{off} decreased to less than 10^{-6} m after the filter converges. The small error in the estimation shown in Fig. 7 depends on the UKF sample time $T_s = 0.05$ s. In fact, simulations show that a reduction of the sample time leads to a reduction of r_e^{off}. Thus, it can be claimed that the offset in the last direction has been correctly
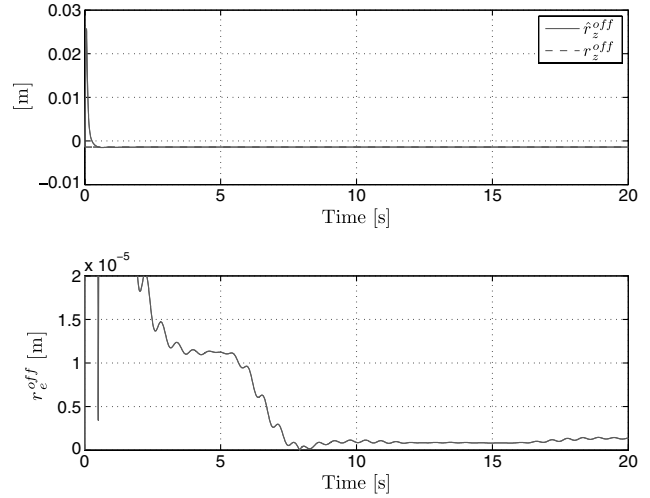

Fig. 7 Simulation results: Top graph shows the estimation of r_z^{off} and the real value. Lower graph shows the estimation error r_e^{off} using UKF.

estimated, and then it can be compensated to drastically reduce the gravitational torque acting on the spacecraft simulator.

To experimentally verify the effectiveness of the automatic balancing procedure proposed here, the following method will be implemented on the CubeTAS. After the balancing procedure, an arbitrary angular velocity will be applied to the system. The total energy, which is the sum of the kinetic energy and the potential energy, is conserved, that is,

$$E_{\text{tot}} = E_r(t) + P_g(t) = \text{constant} \quad (55)$$

where $P_g(t)$ represents the potential energy and $E_r(t) = \frac{1}{2}\omega^T(t)\boldsymbol{J}\omega(t)$ represents the kinetic rotational energy. If the system is balanced, then $P_g(t) \cong 0$. Therefore, the rotational kinetic energy is conserved during the motion, that is, $E_r(t) = E_r(0) = \text{constant}$. Thus the variation of the rotational kinetic energy in time serves as a measure of the effectiveness of the mass balancing procedure. Because the rotational kinetic energy can be evaluated by the gyroscope measurement, this quantity provides an easy way to demonstrate the accuracy of the balance procedure experimentally.

Figure 8 shows the variations of the kinetic energy before and after the balancing procedure. When the system is unbalanced, the variation in amplitude of the kinetic energy will be greater than the amplitude variation with respect to the balanced system. As shown in Fig. 8, the kinetic energy of the unbalanced system has a standard deviation $\sigma^{\text{unbalance}} = 3.847 \times 10^{-3}$ J, where the balanced system has a standard deviation $\sigma^{\text{balance}} = 4.5331 \times 10^{-6}$ J; thus this value
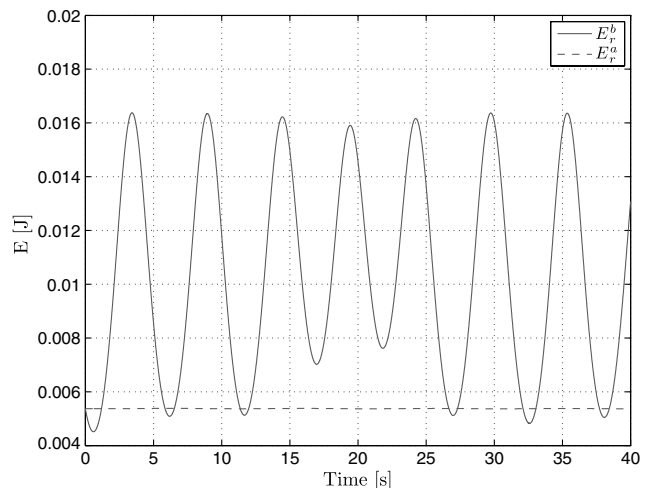

Fig. 8 Simulation results: kinetic energy before E_r^b and after E_r^a the balancing procedure.
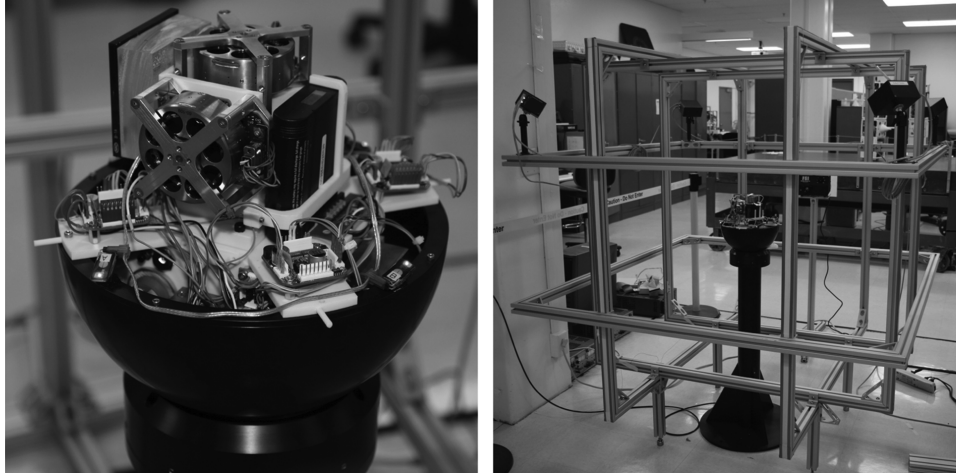
Fig. 9   CubeSat three-axis simulator at the Spacecraft Robotics Laboratory of the Naval Postgraduate School (Lab Director, Marcello Romano).

has been reduced by approximately 99.9%. The value of the standard deviation after balancing procedure is different from zero because the uncertainties in the sliding masses' positions have been modeled as Gaussian white noise distribution. By adding noise into the sliding masses' positions, the system is subjected to a torque that prevents the kinetic energy from being a constant. However, the sensible reduction in the kinetic energy standard deviation is an indication of an effective balance of the system.

V.   Experimental Results

A.   Experimental Apparatus

CubeTAS is a CubeSat-scale three-axis hardware simulator designed to recreate an ideally torque-free platform for testing nanosatellites' attitude determination and control algorithms in a lab environment. The experimental apparatus shown in Fig. 9 has been developed at the Spacecraft Robotics Laboratory of the Naval Postgraduate School.

The CubeTAS simulator contains an automatic balancing system, consisting of three stainless steel masses driven by three linear stepper motors along their axis, respectively. The sliding masses are custom made to encapsulate the stepper motors. The whole system is supported by a spherical air bearing that allows it to rotate ± 50 deg about two axes in the horizontal plane and 360 deg along the vertical axis [24]. A Helmholtz cage has been constructed around the spacecraft simulator to allow the simulation of the orbital magnetic field. Attached to the Helmholtz cage, a high-accuracy motion capture camera system measures the attitude. The main design goal for CubeTAS is to have a shape suitable to be fit in a sphere as shown in Fig. 10. The mechanical design was made such that the offset between the center of mass and the center of rotation is minimum. To meet these goals, the physical shape was designed and the locations

of all the components were determined in three-dimensional (3-D) CAD software NX 7 by Siemens. The property of each component was derived by the CAD file provided by the component's manufacturer. The CubTAS 3-D CAD model is shown in Fig. 10. The upper part is mainly for three reaction wheels and a battery, whereas the lower part is for PC-104 boards, power management boards, and balancing masses with relative linear actuators. The IMU provides information regarding angular velocity and magnetic and gravity fields. A magnetometer, sun sensor, three magnetic coils, and three reaction wheels are used for attitude estimation and control. During the automatic mass balancing experiment, only the data relative to angular velocity and gravity field are used.

B.   Automatic Mass Balancing Experiments

In the first step of the balancing procedure, the offset along the x^b and y^b directions will be compensated. At the beginning of the first experiment, an initial angular velocity of $\boldsymbol{\omega} = [0.0888 \quad 0.8229 \quad 1.3611]^T$ [rad/s] is applied to the spacecraft simulator. As the designed adaptive nonlinear control takes action, the IMU registers the gravity field components and angular velocity values. Shown in Fig. 11 are the gravity field vector components during the rotational motion. It can be seen that, after $t = 200$ s, the only component of the gravity field that is different from zero is the one aligned to the z^b axis. This is in agreement with our theoretical analysis. Figure 12 shows the magnitude of the components of the angular velocity. Solid lines are the experimental results and dashed lines are simulation results. As shown in Fig. 12, the experimental data relative to the magnitude of the angular velocity ω_p tend to zero, so that, at the end of the first step of the balancing procedure, the spacecraft simulator remains to spin only along the z^b axis. This behavior was expected from the simulation results of the proposed balancing method as shown by the dashed lines.
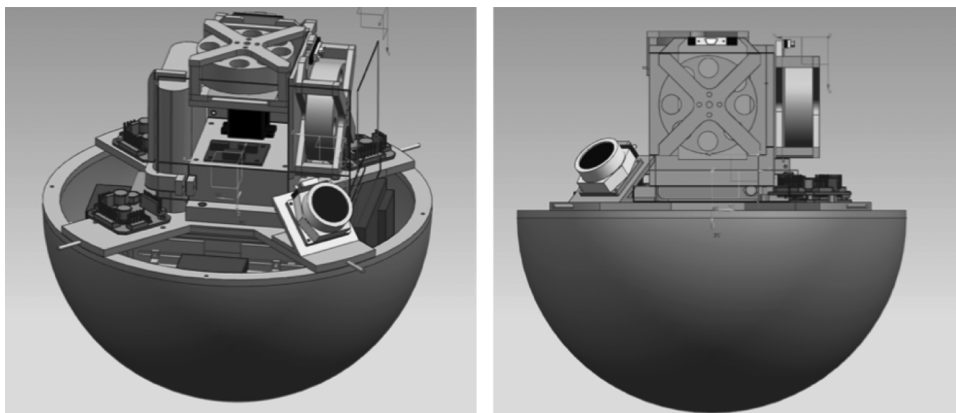

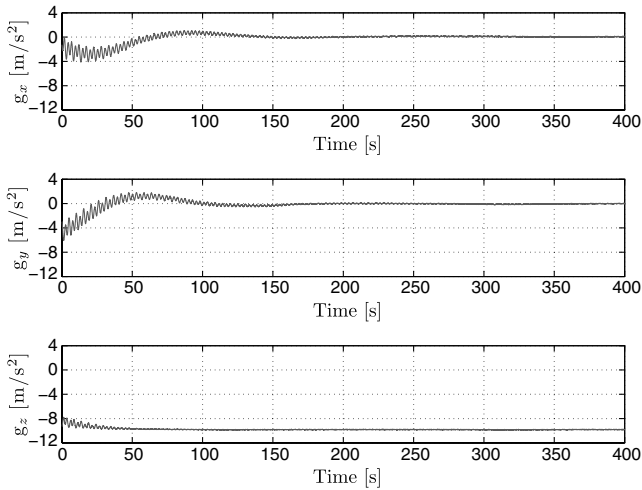Fig. 10   Overview of the CubeTAS body.

Fig. 11 Experimental results: g^b components during transversal balancing procedure.

The discrepancies between experimental and simulation results are particularly evident after $t = 250$ s. In fact, the work of the unmodeled dissipative torque acting on the spacecraft simulator, such as aerodynamic drag, causes the system to lose energy and, consequently, to reduce its angular velocity ω. For this reason, as shown in Fig 12, the experimental value $\|\omega_g\|$ decreases in time instead of converging to a constant. Another difference between experimental and simulation results appears at the beginning of the automatic balancing procedure, where the simulated and experimental systems, under the same control law, react slightly different. Such difference may be caused by unmodeled dynamics. For example, the inner-loop control that adjusts the position of the moving masses to the desired location is not modeled in the simulation. Nevertheless, these discrepancies do not affect the effectiveness of the balancing procedure because, in both cases, the angular velocity $\omega_p \to 0$, as deduced analytically in Eq. (22).

In the second step of the automatic balancing procedure, to compensate the offset in the z^b axis, an unscented Kalman filter is used to estimate the unknown offset. In the experimental validation, the UKF sample time has been set equal to onboard computer sample time $Ts = 0.05$ s. The initial error covariance matrix P_0 has been chosen as

$$P_0 = \mathrm{diag}(0.2^2, 0.2^2, 0.2^2, (2 \times 10^{-3})^2)[\mathrm{rad}^2/\mathrm{s}^2, \mathrm{rad}^2/\mathrm{s}^2, \mathrm{rad}^2/\mathrm{s}^2, \mathrm{m}^2]$$

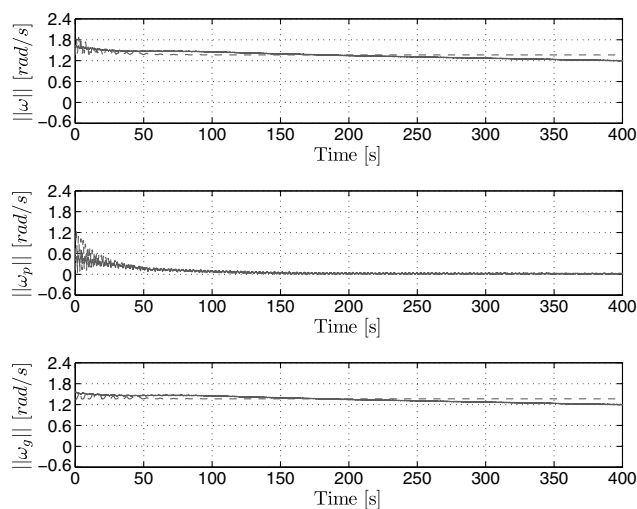**Fig. 12 Experimental and simulation results: Solid lines are experimental data; dashed lines are simulated data of the magnitude of ω, ω_p, and ω_g during transversal balancing procedure.**

so that each diagonal element reflects the square of each experimental initialization error. By analyzing the gyroscope output signal in the steady-state condition, the measurement covariance matrix has been chosen to be

$$\boldsymbol{R} = \mathrm{diag}((0.0024)^2, (0.0021)^2, (0.0027)^2) \ [\mathrm{rad}^2/\mathrm{s}^2]$$

and the associated process noise covariance matrix to be

$$\boldsymbol{Q} = \mathrm{diag}((10^{-4})^2, (10^{-4})^2, (10^{-4})^2, (3 \times 10^{-3})^2)$$
$$\times [\mathrm{rad}^2/\mathrm{s}^4, \mathrm{rad}^2/\mathrm{s}^4, \mathrm{rad}^2/\mathrm{s}^4, \mathrm{m}^2/\mathrm{s}^2]$$

The estimated value of r_z^{off} is shown in Fig. 13. It can be seen that the estimation of the offset in the z^b direction converges to the value of $r_z^{\mathrm{off}} \approx 1.5 \times 10^{-3}$ m. To verify the convergence of the UKF, the square root of the last diagonal element of the error covariance matrix has been plotted. In fact, if the filter operates correctly, this value in time should be as close as possible to zero, as shown in Fig. 13.

The energy conservation method proposed in Sec. IV has been implemented after the mass balancing procedure, to further verify the effectiveness of the balancing method. Before the mass balancing procedure, an angular velocity has been given to the system and the kinetic rotational energy has been recorded. The procedure is repeated after the balancing procedure. Figure 14 shows that the variation in amplitude of the kinetic energy term is drastically reduced after the mass balancing procedure; thus, it is reasonable to conclude that the proposed mass balancing procedure has produced a significant reduction of the offset between the center of mass and the center of rotation. Indeed, the standard deviation has changed from $\sigma^{\mathrm{unbalance}} = 2.8223 \times 10^{-4}$ J to $\sigma^{\mathrm{balance}} = 8.2474 \times 10^{-5}$ J, which is a reduction of $\approx 71\%$. As expected, the reduction in the standard deviation of the kinetic energy is less than the one obtained in the simulation. This is because all the measurements from the IMU relative to angular velocity and gravity field are affected by noise that has not been modeled in the simulation. Furthermore, other dissipative torques that are difficult to simulate affect the spacecraft simulator. The aerodynamic drag is one of the major dissipative torques present during laboratory experimentation. The presence of different wires and components generates an irregular shape that, exposed to the air flow during the rotational motion, produces a dissipative aerodynamic torque that is difficult to model. Nevertheless, by considering low value of angular velocity, the magnitude of the dissipative torque can be considered very small. The presence of these unmodeled dynamics degrades the estimation performance. For this reason, the reduction in the standard deviation of the kinetic energy during the laboratory experimentation is less with respect to the simulated one shown in Fig. 8. In particular, by
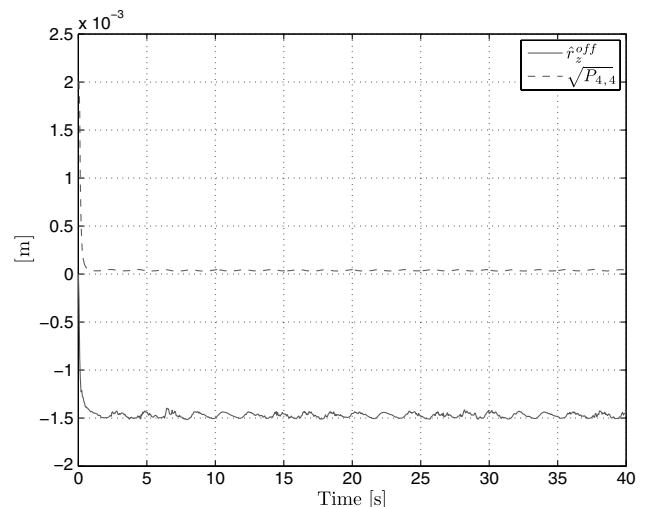

Fig. 13 Experimental results: r_z^{off} estimation using UKF during vertical balancing procedure.
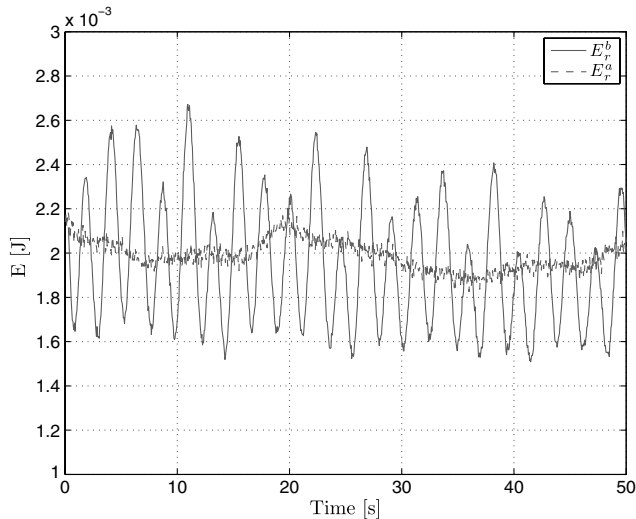
Fig. 14 Experimental results: kinetic energy before E_r^b and after E_r^a the balancing procedure.

observing the energy profile shown in Fig. 14, it is possible to see that the energy tends to decrease in time. This decreasing behavior is due to the work of the dissipative torques that affect the system.

VI. Conclusions

This paper presents an automatic mass balancing system for spacecraft simulators, which allows real-time relocation of the center of mass to the center of rotation using only sliding masses. Compared with manual balancing, the proposed automatic balancing system can greatly reduce the labor involved in the balancing process and save design time. The use of sliding masses as the only actuator makes the implementation relatively easy and the proposed automatic balancing system suitable for small-size spacecraft simulators. To overcome the physical limitation of the actuator (i.e., the torque generated by moving masses is constrained in the direction perpendicular to the gravity field), a two-step design is proposed. The performance of the proposed automatic balancing method is theoretically justified using Lyapunov stability analysis and is demonstrated at simulation level. The experiment conducted on a CubeSat-scale simulator also shows the efficacy of the proposed method; however, the presence of unmodeled dynamics (e.g., aerodynamic drag) and different sources of noise degrades the performance. Further work is needed to incorporate dissipative torques and to analyze the effect of various noises to improve the accuracy.

References

[1] Kim, B. M., Velenis, E., Kriengsiri, P., and Tsiotras, P., "Designing a Low-Cost Spacecraft Simulator," *IEEE Control Systems*, Vol. 34, No. 4, Aug. 2003, pp. 26–37.

[2] Schwartz, J. L., Peck, M. A., and Hall, C. D., "Historical Review of Air Bearing Spacecraft Simulators," *Journal of Guidance, Control, and Dynamics*, Vol. 26, No. 4, 2003, pp. 513–522. doi:10.2514/2.5085

[3] Smith, G. A., "Dynamic Simulators for Test of Space Vehicle Attitude Control System," *Proceedings of the Conference on the Role of Simulation in Space Technology, Part C*, Virginia Polytechnic Inst. and State Univ., Blacksburg, VA, Aug. 1964.

[4] Fullmer, R. R., "Dynamic Ground Testing of the Skipper Attitude Control System," *34th AIAA Aerospace Science Meeting and Exhibit*, AIAA Paper 1996-0103, Jan. 1996.

[5] Peck, M. A., and Cavender, A. R., "Airbearing-Based Testbed for Momentum Control Systems and Spacecraft Line of Sight," *13th Annual AAS/AIAA Spaceflight Mechanics Meeting*, American Astronautical Society Paper 03-127, Feb. 2003.

[6] Romano, M., and Agrawal, B. N., "Acquisition, Tracking and Pointing Control of the Bifocal Relay Mirror Spacecraft," *Acta Astronautica*, Vol. 53, No. 4, 2003, pp. 509–519. doi:10.1016/S0094-5765(03)80011-5

[7] Kim, J. J., and Agrawal, B. N., "Automatic Mass Balancing of Air-Bearing-Based Three-Axis Rotational Spacecraft Simulator," *Journal of Guidance, Control, and Dynamics*, Vol. 32, No. 3, 2009, pp. 1005–1017. doi:10.2514/1.34437

[8] Prado, J., Bisiacchi, G., Reyes, L., Vicenta, E., Contreras, F., Mesinas, M., and Juarez, A., "Three-Axis Air-Bearing Based Platform for Small Satellite Attitude Determination and Control Simulation," *Journal of Applied Research and Technology*, Vol. 3, No. 3, Dec. 2005, pp. 222–237.

[9] Prado, J., and Bisiacchi, G., "Dynamic Balancing for a Satellite Attitude Control Simulator. Instrumentation and Development," *Journal of the Mexican Society of Instrumentation*, Vol. 4, No. 5, 2000, pp. 76–81.

[10] Hatcher, N. M., and Young, R. N., "Automatic Balancing System for Use on Frictionlessly Supported Attitude-Controlled Test Platforms," NASA TN-D-4426, Langley Research Center, March 1968.

[11] Yang, Y., and Cao, X., "Design and Development of the Small Satellite Attitude Control System Simulator," *AIAA Modeling and Simulation Technologies Conference and Exhibit*, AIAA Paper 2006-6124, Keystone, CO, Aug. 2006.

[12] Li, Y., and Gao, Y., "Equations of Motion for the Automatic Balancing System of 3-DOF Spacecraft Attitude Control Simulator," *Third International Symposium on Systems and Control in Aeronautics and Astronautics (ISSCAA)*, IEEE, June 2010, pp. 248–251.

[13] Jung, D., and Tsiotras, P., "3-DoF Experimental Test-Bed for Integrated Attitude Dynamics and Control Research," AIAA Paper 2003-5331, Aug. 2003.

[14] Schwartz, J. L., and Hall, C. D., "System Identification of a Spherical Air-Bearing Spacecraft Simulator," AAS Paper 2004-122, Feb. 2004.

[15] Woo, H., Perez, O. R., Chesi, S., and Romano, M., "CubeSat Three Axis Simulator (CubeTAS)," *Proceedings of the AIAA Modeling and Simulation Technologies Conference*, AIAA Paper No. 2011-6271, Aug. 2011.

[16] Likins, P. W., *Elements of Engineering Mechanics*, McGraw–Hill, New York, 1973, pp. 438–439.

[17] Leine, R. I., and Wouw, N., "Stability and Convergence of Mechanical Systems with Unilateral Constraints," *Lecture Notes in Applied and Computational Mechanics*, Vol. 36, Springer, New York, 2008, pp. 145–148.

[18] Crassidis, J., and Markley, F., "Unscented Filtering for Spacecraft Attitude Estimation," *Journal of Guidance, Control, and Dynamics*, Vol. 26, No. 4, 2003, pp. 536–542. doi:10.2514/2.5102

[19] Julier, J., and Uhlmann, J. K., "A New Extension of the Kalman Filter to Nonlinear Systems," *Signal Processing, Sensor Fusion, and Target Recognition VI*, Vol. 3068, 1997, pp. 182–193.

[20] Matthew, C. V., Schwartz, J. L., and Christopher, D. H., "Unscented Kalman Filtering for Spacecraft Attitude State and Parameter Estimation," *Proceedings of the AAS/AIAA Space Flight Mechanics Conference*, AAS Paper 04-115, 2005.

[21] Sekhavat, P., Gong, Q., and Ross, I. M., "NPSAT1 Parameter Estimation Using Unscented Kalman Filtering," *Proceedings of the American Control Conference*, IEEE, Piscataway, NJ, July 2007, pp. 4445–4451.

[22] Simon, D., *Optimal State Estimation: Kalman, H∞, and Nonlinear Approaches*, Wiley, Hoboken, NJ, 2006, pp. 403–407.

[23] Kang, W., and Barbot, J.-P., "Discussions on Observability and Invertibility," *Seventh IFAC Symposium on Nonlinear Control Systems*, Aug. 2007.

[24] Chesi, S., Pellegrini, V., Gong, Q., Cristi, R., and Romano, M., "Automatic Mass Balancing for Small Three-Axis Spacecraft Simulator Using Sliding Masses Only," *Advances in the Astronautical Sciences*, Vol. 142, No. 3, 2012, pp. 2547–2562.